Preprints of the
9th International Symposium on Advanced Control of Chemical Processes
The International Federation of Automatic Control
June 7-10, 2015, Whistler, British Columbia, Canada

Model predictive control of the steam cycle in a solar power plant ⋆

Dominik Mier *, **Florian Möllenbruck** *, **Michael Jost** *,
Wolfgang Grote **, **Martin Mönnigmann** *

* *Automatic Control and Systems Theory, Ruhr-Universität Bochum, Bochum, Germany*
** *MAN Diesel & Turbo SE, Oberhausen, Germany*

Abstract: We derive a nonlinear model of the steam cycle of a solar power plant, estimate its unknown parameters with measured data, and design a linear model predictive controller based on the resulting model. Simulations show that the linear model predictive controller is able to regulate the electrical power of the nonlinear steam process of the plant to a given reference trajectory very well. Moreover, it results in very good disturbance rejection.

Keywords: Power plant control, solar power, model predictive control

1. INTRODUCTION

Various types of solar power plants are established (see Camacho et al. (2010) for a summary). We consider a parabolic trough solar power plant. Plants of this type are based on concentrating the solar irradiation onto an absorber pipe positioned in the focal line of a parabolic mirror. A heat transfer fluid (HTF) circulating inside the absorber pipe supplies energy to a heat exchanger, where it is used to generate steam. The steam is passed into a multi-group steam turbine, which drives a synchronous generator. Systems of this type are known to pose complex control problems. Many researchers have considered the oil circuit in detail, see the survey articles Camacho et al. (2007a,b) and references therein for an overview. We here focus on the steam part of the plant, which consists of a steam turbine, a generator and a condenser. These subsystems show fast dynamical and nonlinear behavior and are sensitive to disturbances, which therefore must be accounted for in the modeling and in the control concept.

We use nonlinear models based on those given in Jost et al. (2014), but include more details in the models presented here. Transient data recorded in a real solar power plant were used to adjust the unknown parameters. The resulting models have been verified with independent recorded data. In contrast to those given in Jost et al. (2014) the models that result here are shown to be accurate even for transient operations.

We present a model of the plant in Sect. 2. We then use logged measurement data to estimate unknown parameters such as efficiency factors and heat transfer coefficients (Sect. 3). The resulting model is used to set up a model predictive controller for the steam cycle of the plant in Sect. 4. Simulation results for the controlled nonlinear system are presented in Sect. 5. Conclusions and an outlook are stated in Sect. 6.

2. PHYSICAL MODEL

A sketch of the steam cycle of the solar power plant is shown in Fig. 1. We present detailed models of the steam turbine and the condenser in Sections 2.1 and 2.2, respectively. Models of the remaining subsystems, specifically the generator, feedwater pump and the steam generator, are summarized in Sect. 2.3.

2.1 Turbine

A schematic representation of the turbine is given in Fig. 2. The steam turbine is modeled as a two group extraction turbine with pre- and reheater.

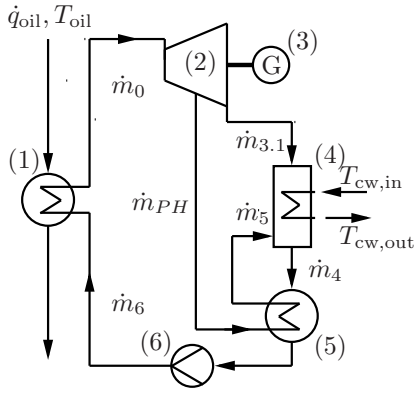

Fig. 1. Sketch of the steam cycle: Feed water is evaporated and superheated in a steam generator (1) and passed into the turbine (2). Several bleeds (steam extractions from the turbine) are summarized in the mass flow $\dot{m}_{PH}$ and used to preheat (5) the feedwater. The remaining steam expands in the low pressure turbine and is condensed by a water condenser (4). Via the feed pump (6), the condensate is supplied to the boiler again. A generator (3) is coupled to the turbine to convert the mechanical power into electric power.

⋆ Support by the European Union under the European Regional Development Fund is gratefully acknowledged.

EUROPEAN UNION
Investing in our Future
European Regional Development Fund
Ziel2.NRW
Regionale Wettbewerbsfähigkeit und Beschäftigung
Ministerium für Innovation, Wissenschaft und Forschung des Landes Nordrhein-Westfalen

The inlet mass flow rate $\dot{m}_1$ through the nozzle groups of the turbine can be controlled by the control valve position u_V. The characteristics of this valve can be described by

$$\dot{m}_1 = \dot{m}_0 \sqrt{\frac{p_0 T_{0,0}}{T_0 p_{0,0}}} (3u_V^2 - 2u_V^3), \tag{1}$$

where $T_{0,0}$ and $p_{0,0}$ denote the design point of live steam temperature and pressure, respectively (Grote, 2009, p. 78).

The mass flow rate through a turbine group is a function of the inlet pressure, outlet pressure and the temperature T_1 of the inlet steam. For the high-pressure (HP) group of the turbine the flow rate can be described by

$$\dot{m}_2 = K_{ST} \sqrt{\frac{p_1^2 - p_2^2}{T_1}}. \tag{2}$$

This relation, which is known as Stodola's law of the ellipse, permits calculating power and steam flow rates for off-design operation points (for example, for part load conditions of turbine sections). The constant K_{ST} can be determined from the nominal design parameters. For the HP turbine this yields

$$K_{ST} = \dot{m}_0 \sqrt{\frac{T_{1,0}}{p_{1,0}^2 - p_{2,0}^2}}. \tag{3}$$

Equations (2) and (3) also apply to the low pressure group of the turbine with the respective pressures and specific volumes. To the knowledge of the authors no suitable model for the leakage mass flow rate through the labyrinth seals of the turbine $\dot{m}_{LF}$ exists. We therefore use design data obtained from the turbine manufacturer to approximate $\dot{m}_{LF}$ as a function of the inlet pressure of the HP group. The empirical relation

$$\dot{m}_{LF} = 0.0042 p_1^{1.0326} \tag{4}$$

results from this approach.

Applying the conservation-of-mass-principle to a steam chamber leads to an ordinary differential equation for the chamber pressure. The resulting equation for the outlet pressure of the HP turbine, for example, reads

$$\dot{p}_2 = \frac{c^2}{V_2} \cdot (\dot{m}_{2.1} - \dot{m}_{2.2} - \dot{m}_3), \tag{5}$$

where $\dot{m}_{2.1} = \dot{m}_2 - \dot{m}_{LF}$, and where c is the instantaneous sonic speed of the steam inside the volume V_2. The pressure dynamics after the low pressure group are included in the condenser model. The dynamics of the pipe flows are neglected for simplicity. The bleed mass flow in the low pressure group $\dot{m}_{3,T}$ and the mass flow rate $\dot{m}_{2.2}$ (see Fig. 2) are also approximated by empirical relations that are derived from manufacturer design data. The resulting expressions read

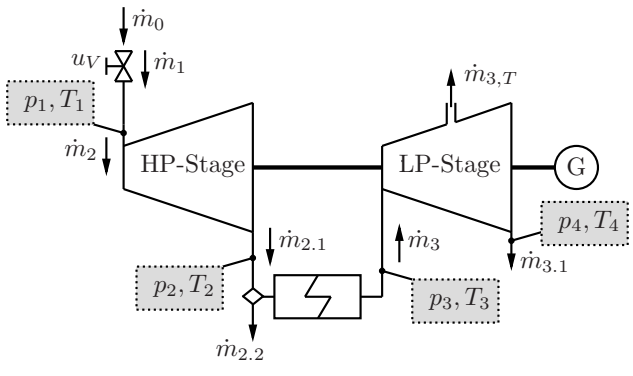

Fig. 2. Schematic representation of the turbine

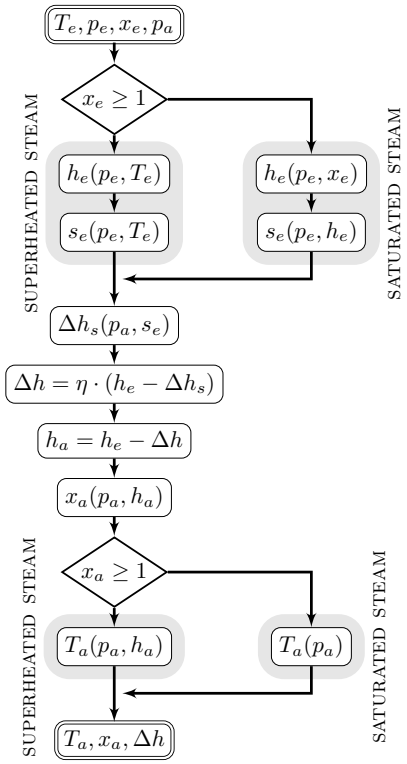

Fig. 3. Polytropic expansion (Grote, 2009, p. 52)

$$\dot{m}_{3,T} = 0.0065 p_3^2 + 0.04351 p_3 - 0.5393 \tag{6}$$

and

$$\dot{m}_{2.2} = 0.0021 p_1^{1.8812}, \tag{7}$$

respectively.

The total mass flow $\dot{m}_{PH}$ consumed by the pre-heaters is

$$\dot{m}_{PH} = \dot{m}_{2.2} + \dot{m}_{3,T}. \tag{8}$$

Thermodynamic steam properties are calculated with the IAPWS-IF97 formulas (Wagner and Kretzschmar, 1997). The algorithm used to calculate the polytropic expansion in steam turbines is shown in Fig. 3. The calculation must be performed for all turbine stages. Specifically, it must be carried out for both the HP and LP section.

The thermal power is obtained from

$$P = P_{HP} + P_{LP} \tag{9}$$

with

$$P_{HP} = (\dot{m}_2 - \dot{m}_{LF})\,(\eta \Delta h_{HP})\,,$$
$$P_{LP} = (\dot{m}_3 - \dot{m}_{3,T} \cdot w)\,(\eta \Delta h_{LP})\,,$$

where w is the fraction of extracted steam, Δh_{HP} and Δh_{LP} are the enthalpy difference for the high pressure and low pressure stage, respectively, and η is the isentropic efficiency.

2.2 Condenser

The steam enters a condenser after passing the LP turbine. The exhaust steam pressure dynamics can also be modeled

with a single lumped, ideally mixed volume. This yields

$$\dot{p}_4 = \frac{c^2}{V_\mathrm{C}}(\dot{m}_3 - \dot{m}_{3,T} - \dot{m}_4), \tag{10}$$

where V_C is the sum of the steam volumes in the condenser and the exhaust pipe of the turbine. The mass flow of the condensing steam $\dot{m}_4$ can be calculated from the latent heat of vaporization h_r and the heat flow Q according to

$$\dot{m}_4 = \frac{Q}{h_r}, \tag{11}$$

where h_r is given by

$$h_r = a_1 + a_2 \cdot \ln p_4 + a_3 \cdot (\ln p_4)^2, \quad p_4 \in [0.01, 1].$$

The heat flow Q reads

$$Q = kA \cdot \frac{T_{\mathrm{cw,out}} - T_{\mathrm{cw,in}}}{\ln \frac{T_4 - T_{\mathrm{cw,in}}}{T_4 - T_{\mathrm{cw,out}}}}, \tag{12}$$

where $T_{\mathrm{cw,out}}$ and $T_{\mathrm{cw,in}}$ are the cooling water temperature at the outlet and inlet, respectively. The heat transfer coefficient kA depends on the mass flow of exhaust steam, since the heat transfer of film condensing improves as the mass flow of the condensate increases. However, a saturation effect must be considered. Assuming that the heat transfer from the steam to the cooling water is dominated by film condensation on the surfaces of the condenser pipes the relation $Nu = l \cdot Re^n \cdot Pr^m$ holds for the Nusselt number, where Re is the Reynolds number, Pr is the Prandtl number and l, n and m are problem-specific constants (Incropera et al., 2007). With $Nu \propto kA$, $Re \propto \dot{m}_4$ and $Pr \approx$ const., it is reasonable to describe the heat transfer coefficient by

$$kA = b_2 \dot{m}_4^{b_1}, \tag{13}$$

where b_2 and $b_1 \approx 0.38$ for film condensation are determined from measured data. The exhaust steam temperature can be calculated with Magnus's formula

$$T_4 = \frac{c_2 \ln\left(\frac{p_4}{c_0}\right)}{c_1 - \ln\left(\frac{p_4}{c_0}\right)} + 273.15, \tag{14}$$

where c_0, c_1 and c_2 are specific constants (Alduchov and Eskridge, 1996). The dynamics of the effluent cooling water follow from the first law of thermodynamics and read

$$\dot{T}_{\mathrm{cw,out}} = \frac{2\dot{m}_w}{m_w}(T_{\mathrm{cw,in}} - T_{\mathrm{cw,out}}) + \frac{2}{m_w c_p} Q, \tag{15}$$

where $\dot{m}_w$ is the mass flow and m_w is the mass of the cooling water and c_p is the specific heat capacity.

2.3 Equations of the auxiliary subsystems

We briefly summarize the equations for the remaining components. For more details we refer to Jost et al. (2014) and the references therein. Indices "in" and "out" are used to refer to the input state and the output state, respectively.

Feedwater pump: The pressure difference between the inlet and outlet is given by

$$\Delta p = \left(\frac{n}{n_0}\right)^2 d_0 + \left(\frac{n}{n_0}\right) d_1 \dot{q} + d_2 \dot{q}^2, \tag{16}$$

where d_0, d_1 and d_2 are constants, n_0 denotes the nominal rotational speed, n is the instantaneous rotary speed of the pump and $\dot{q}$ is the volume flow rate (Gülich, 2010; Leonow and Mönnigmann, 2013).

Generator: The equations for the rotor dynamics and the power output read

$$\begin{aligned} \ddot{\varphi} &= \frac{1}{\theta}(M_\mathrm{I} - M_\mathrm{T}\sin(\varphi) - d_\mathrm{e}\dot{\varphi}), \\ P_\mathrm{el} &= M_\mathrm{T}\sin(\varphi) 2\pi f_0, \end{aligned} \tag{17}$$

respectively, where φ is the rotor angle, d_e is a damping constant, M_T is the tilting torque of the machine, θ is the inertia torque and f_0 is the nominal grid frequency (Chapman, 2012).

Preheater/Superheater: The differential equations for the output temperatures read

$$\begin{aligned} \dot{T}_{\mathrm{P,out}} = &\frac{\dot{m}_{\mathrm{P,out}}}{m_{\mathrm{P,out}}}(T_{\mathrm{P,in}} - T_{\mathrm{P,out}}) \\ &- \frac{kA}{m_{\mathrm{P,out}} c} \Delta\vartheta_{\log}(T_{\mathrm{P,out}} - T_{\mathrm{w,in}}, T_{\mathrm{P,in}} - T_{\mathrm{w,out}}) \end{aligned} \tag{18}$$

where $T_{\mathrm{P,in}}$, $T_{\mathrm{P,out}}$ denote the steam inlet and outlet temperatures and $T_{\mathrm{w,in}}$, $T_{\mathrm{w,out}}$ refer to the feedwater inlet and outlet temperatures; and $\Delta\vartheta_{\log}(T_{\mathrm{P,out}} - T_{\mathrm{w,in}}, T_{\mathrm{P,in}} - T_{\mathrm{w,out}})$ is the logarithmic temperature difference (Incropera et al., 2007, p. 670) which is defined by

$$\Delta\vartheta_{\log}(\Delta T_\mathrm{A}, \Delta T_\mathrm{B}) = \begin{cases} \dfrac{\Delta T_\mathrm{A} - \Delta T_\mathrm{B}}{\ln(\Delta T_\mathrm{A}) - \ln(\Delta T_\mathrm{B})}, & \Delta T_\mathrm{A}\Delta T_\mathrm{B} > 0, \\ 0, & \text{otherwise.} \end{cases} \tag{19}$$

The pressures in the heaters can be described by

$$\dot{p}_\mathrm{P} = \frac{c^2}{V_\mathrm{P}}(\dot{m}_{PH} - \dot{m}_{\mathrm{P,out}}), \tag{20}$$

where c is the sonic speed, V_P is the volume and $\dot{m}_{\mathrm{P,out}}$ is given by

$$\dot{m}_{\mathrm{P,out}} = \left(\frac{p_\mathrm{in} - p_\mathrm{P}}{R}\right)^{\frac{4}{7}}, \tag{21}$$

see Jost et al. (2014) for more details.

Evaporator: The differential equation for the output temperature reads

$$\begin{aligned} \dot{T}_{\mathrm{E,out}} = &\frac{2\dot{m}_{\mathrm{E,out}}}{m_{\mathrm{E,out}}}(T_{\mathrm{E,in}} - T_{\mathrm{E,out}}) \\ &- \frac{2kA}{m_{\mathrm{E,out}} c_\mathrm{p}} \Delta\vartheta_{\log}(T_{\mathrm{E,out}} - T_{\mathrm{w,in}}, T_{\mathrm{E,in}} - T_{\mathrm{w,out}}), \end{aligned} \tag{22}$$

where the temperatures and the logarithmic temperature difference are defined as before. The mass flow is given by

$$\dot{m}_{\mathrm{E,in}} = \frac{kA}{h_\mathrm{E}} \Delta\vartheta_{\log}(T_{\mathrm{E,out}} - T_{\mathrm{w,in}}, T_{\mathrm{E,in}} - T_{\mathrm{w},in}) \tag{23}$$

where h_E is the enthalpy of the vaporized water (Sonntag and Van Wylen, 1971, p. 140). The pressure and the mass flow in the evaporator can be described by (20) and (21).

Combining (1)–(23) results in a nonlinear state space model of the steam cycle sketched in Fig. 1, which has the form

$$\begin{aligned} \dot{x} &= f(x, u, \Omega, z), \\ y &= h(x, \Omega), \end{aligned} \tag{24}$$

with state vector is $x = (p_2, p_4, \varphi, \dot{\varphi}, T_{\mathrm{cw,out}}, T_{\mathrm{P,out}}, p_{\mathrm{P,in}}, T_{\mathrm{E,out}}, p_{\mathrm{E,in}})'$, input vector $u = (u_\mathrm{V}, n)'$, output $y = P_\mathrm{el}$, and disturbance $z = T_{\mathrm{cw,in}}$. Ω denotes the parameter vector which includes all parameters of the steam part. We state (24) in Appendix A.

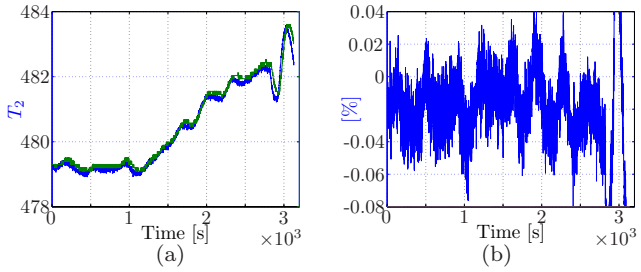

Fig. 4. Comparison of the measured temperature values T_2 and the corresponding simulation results: (a) blue curve shows simulation results, green curve shows measured values. (b) percentage relative difference between measured and simulated data.

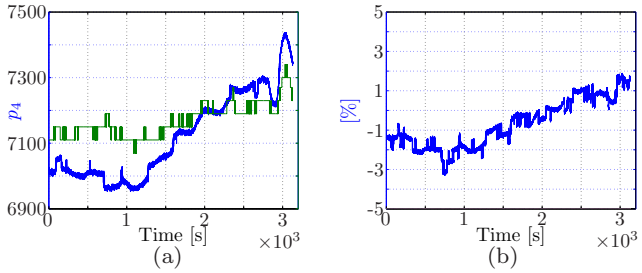

Fig. 5. Comparison of the measured pressure values p_4 and the corresponding simulation results: (a) blue curve shows simulation results, green curve shows measured values. (b) percentage relative difference between measured and simulated data.

3. PARAMETER ESTIMATION AND MODEL VERIFICATION

We use data measured in an industrial solar power plant to adjust unknown model parameters in a submodel of (24), specifically, in the models of the turbine, condenser and the generator. This submodel is shown in Fig. 2, where the measured physical quantities are highlighted with gray boxes. Data have been logged with a sampling time of 20 milliseconds with data acquisition software we developed for communication with the plant controller.

The subsystems turbine, condenser and generator are described by (5) and Fig. 3, Eqs. (10) and (15) and (9), respectively. Together these equations define the nonlinear state space model

$$\begin{aligned} \dot{\bar{x}} &= \bar{f}(\bar{x}, \bar{u}, \bar{\Omega}, z), \\ \bar{y} &= \bar{h}(\bar{x}, \bar{\Omega}), \end{aligned} \tag{25}$$

with state vector $\bar{x} = (p_2, p_4, \varphi, \dot{\varphi}, T_{\mathrm{cw,out}})'$, measured signals $\bar{u} = (p_1, T_1, T_3)'$, system output $\bar{y} = (p_2, p_4, T_2, T_4, P_{\mathrm{el}}, T_{\mathrm{cw,out}})'$, measured disturbance $z = T_{\mathrm{cw,in}}$ and parameter vector $\bar{\Omega} = (\eta, b_1, b_2, m_w, \dot{m}_w, w)'$. Note that the measured signals $\bar{u}$ are not the inputs of the full model (24), but merely the signals that are available for the parameter estimation. All parameters not mentioned here are chosen as in Jost et al. (2014).

We describe the parameter estimation in Sect. 3.1 and verify the models with independent data in Sect. 3.2.

3.1 Parameter Estimation

We estimate the isentropic efficiency η (cf. (9)), the coefficients b_1 and b_2 of the heat transfer equation (cf. (13)), the mass m_w and the mass flow $\dot{m}_w$ of the cooling water (cf. (15)) and the factor w (cf. (9)) that describe the influence of the bleeds on the thermal power.

Parameters are estimated by solving the nonlinear least squares problem

$$\begin{aligned} \min_{\bar{\Omega}} \quad & \sum_{k=1}^{N} \left(\tilde{y}(k) - y(k, \bar{\Omega})\right)^2 \\ \text{s.t.} \quad & \dot{\bar{x}} = f(\bar{x}, \bar{u}(k), \bar{\Omega}, z(k)), \\ & \bar{y} = \bar{h}(\bar{x}, \bar{\Omega}), \\ & \bar{\Omega}^- \le \bar{\Omega} \le \bar{\Omega}^+, \end{aligned} \tag{26}$$

where the output $\tilde{y}(k)$, the signals $\bar{u}(k)$ and disturbance $z(k)$ are available from measurements at times t_k, $k = 1, \ldots, N$. The number of sample points is $N = 10^6$, which corresponds to a time span of approximately half an hour. The prediction-error minimization algorithm (pem) provided by the Matlab System Identification Toolbox was used to obtain the optimal solution $\bar{\Omega}^\star$ of (26).

3.2 Model verification

We verify the resulting nonlinear state space model (25) by comparing the system outputs $\bar{y}(k, \bar{\Omega}^\star)$ to data measured independently of the time series used to determine the optimal parameters $\bar{\Omega}^\star$. We show the results for the outlet pressure p_4 of the LP-Stage (cf. (10)) and the outlet temperature of the HP-Stage T_2 (cf. Alg. 3) in Figs. 5 and 4, respectively. We select these quantities, because the smallest (T_2) and the largest (p_4) percentage root mean square error x_{rms} result for them, where x_{rms} is defined by

$$x_{\mathrm{rms}} = \sqrt{\frac{1}{N}\left(\sum_{k=1}^{N}\left(\frac{\tilde{y}(k) - y(k, \bar{\Omega}^\star)}{\tilde{y}(k)} \cdot 100\%\right)^2\right)}. \tag{27}$$

Root mean square errors for the remaining outputs of the subsystems, specifically P_{el}, T_4, p_2, $T_{\mathrm{cw,out}}$, are listed in Tab. 1. The largest error amounts to 1.4079%. It occurs for the outlet pressure p_4 of the LP-Stage. We infer the models presented in Sect. 2 with the parameters estimated in Sect. 3.1 are accurate enough for controller design and tuning.

4. MODEL PREDICTIVE CONTROL

We give a brief introduction to MPC in Sect. 4.1 and present details on the specific controller used here in Sect. 4.2.

Component	Output y_i	$x_{\mathrm{rms},i}$ in %
HP-Stage	p_2	0.1211
	T_2	0.0346
LP-Stage	T_4	0.1753
Generator	P_{el}	0.7736
Condenser	p_4	1.4079
	$T_{\mathrm{cw,out}}$	0.1231

Table 1. Root mean squared error x_{rms} for all outputs. Note that the largest value is only $x_{\mathrm{rms}} = 1.4079\%$ (for p_4); and four out of six figures are smaller than 0.18%

4.1 Brief introduction to model predictive control

We assume the nonlinear state space model (24) derived in Sect. 2 has been linearized at a point of operation (x_0, u_0) and discretized. This yields a linear discrete-time state space system of the form

$$\begin{aligned} \hat{x}(k+1) &= A\hat{x}(k) + B\hat{u}(k),\ \hat{x}(0) = \hat{x}_0 \\ \hat{y}(k) &= C\hat{x}(k) + D\hat{u}(k) \end{aligned} \tag{28}$$

with states $x \in \mathbb{R}^n$, inputs $u \in \mathbb{R}^m$, outputs $y \in \mathbb{R}^p$ and constraints

$$\begin{aligned} \hat{u}_{\min} \le \hat{u}(k) \le \hat{u}_{\max}, \\ \hat{y}_{\min} \le \hat{y}(k) \le \hat{y}_{\max}, \end{aligned} \tag{29}$$

for all $k \ge 0$, where $\hat{u}_{\min}$, $\hat{u}_{\max}$, $\hat{y}_{\min}$ and $\hat{y}_{\max}$ are of appropriate dimensions and $\hat{u}_{\min} < 0 < \hat{u}_{\max}$, $\hat{y}_{\min} < 0 < \hat{y}_{\max}$. Symbols with a hat refer to differences w.r.t. the point of linearization, for example, $\hat{x}(t) = x(t) - x_0$.

MPC seeks an input sequence that essentially minimizes the deviation between the system output $\hat{y}(k)$ and a reference trajectory $\hat{w}(k)$ by solving the optimal control problem

$$\begin{aligned} \min_{U,Y} \quad & \sum_{j=1}^{H_p} \|\hat{y}(k+j) - \hat{w}(k+j)\|^2_{Q_{\hat{y}}} + \sum_{j=0}^{H_p-1} \|\hat{u}(k+j)\|^2_{R_{\hat{u}}}, \\ \text{s.t.} \quad & \hat{x}(k+1) = A\hat{x}(k) + B\hat{u}(k), \\ & \hat{y}(k) = C\hat{x}(k) + D\hat{u}(k), \\ & \hat{u}_{\min} \le \hat{u}(k) \le \hat{u}_{\max}, \\ & \hat{y}_{\min} \le \hat{y}(k) \le \hat{y}_{\max}, \end{aligned} \tag{30}$$

where $U' = [\hat{u}(k)', \ldots, \hat{u}(k+H_p)']$, $Y' = [\hat{y}(k)', \ldots, \hat{y}(k+H_p)']$; and where $\|v\|^2_M$ is short for $v'Mv$. In (30), $R_{\hat{u}}$ and $Q_{\hat{y}}$ denote the weighting matrices on the inputs and the output error, respectively, and H_p denotes the horizon.

We use several extensions to the basic model predictive control formulation (30), which can be summarized as follows. Weightings on the rate of change of the input $R_{\Delta\hat{u}}$ and rate constraints can be considered in (30) by augmenting the state with the input of the current time step and introducing the difference $\Delta\hat{u} = \hat{u}(k) - \hat{u}(k-1)$ as an artificial system input (see e.g. Maciejowski (2002, Chpt. 2.2, p. 41)). If the system is subject to state and output disturbances an observer has to be included in the problem formulation (30) to regulate the output error $\hat{y}(k) - w(k)$ to zero. We choose the observer gain matrices for the states and disturbances as zero and unitiy matrix, respectively, see e.g. Maciejowski (2002, Chpt. 2.6.3, p. 57), see also Grote (2009, Chpt. 4.2.2, p. 131). For the considered stable plant, stability of the closed loop can be obtained with an appropriate choice of Q_y and R_u (see e.g. Maciejowski (2002, Chpt. 6, p. 167)).

4.2 Controller design

Linearization of the model described in Sect. 2 results in a stable discrete-time model of the form (28) with 10 states, 2 inputs (control valve $\hat{u}_V = u_V - u_{V,0}$, cf. (1); speed of feedwater pump $\hat{n} = n - n_0$, cf. (16)) and one output (generated power $\hat{P}_{\text{el}} = P_{\text{el}} - P_{\text{el},0}$, cf. (17)). The sample time was set to $T_s = 0.1$s. We removed 4 uncontrollable states to obtain a suitable model for controller design,

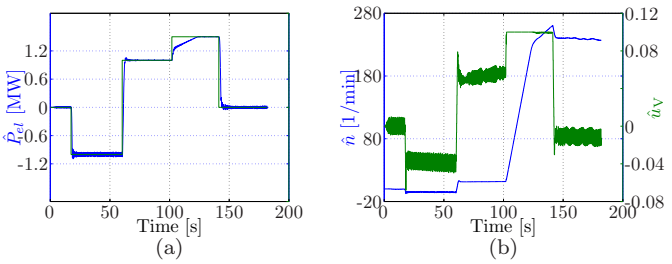

Fig. 6. Results for the set point change: (a) blue curve shows the simulated electric power, green curve shows the set point. (b) inputs of the system; blue curve corresponds to the speed of the feedwater pump, green curve corresponds to the valve position.

which results in a discrete-time state space model of form (28) with 6 states.

The following output, input and rate constraints were applied

$$\begin{aligned} -10 \cdot 10^6 \le\ & \hat{y}(t) && \le 10 \cdot 10^6, \\ \begin{pmatrix} -0.9 \\ -1000 \end{pmatrix} \le\ & \hat{u}(t) && \le \begin{pmatrix} 0.1 \\ 1000 \end{pmatrix}, \\ \begin{pmatrix} -0.01 \\ -1 \end{pmatrix} \le\ & \Delta\hat{u}(t) && \le \begin{pmatrix} 0.01 \\ 1 \end{pmatrix}. \end{aligned}$$

The weighting matrices are chosen to be $Q_y = 10^{-4}$, $R_u = 0$, $R_{\Delta u} = 10^4 \cdot I^{2\times 2}$ and the prediction horizon is set to $H_p = 50$. The resulting quadratic program has 500 constraints and 100 decision variables.

5. SIMULATION AND RESULTS

We simulate the steam part of the power plant for several operation conditions to assess the performance of the proposed controller. We stress that all simulations are carried out with the nonlinear models described in Sect. 2. For simplicity we made the following assumptions throughout the simulations: (a) piping dynamics are neglected, (b) oil temperature and flow rate at the steam generator inlet are constant, i.e. the oil part of the plant is in steady state, (c) the mass flow $\dot{m}_{\text{PH}}$ is not controlled and depends on the pressures p_2 and p_3 only, and (d) the reheater is not controlled.

We assess the controller performance with the following two scenarios.

Set point change: We apply the following reference trajectory to the output $\hat{y} = \hat{P}_{\text{el}}$ in (30).

- $\Delta 0$ MW $\to -\Delta 1$ MW at time $t_1 = 17.5s$,
- $-\Delta 1$ MW $\to \Delta 1$ MW at time $t_2 = 60s$,
- $\Delta 1$ MW $\to \Delta 1.5$ MW at time $t_3 = 102s$,
- $\Delta 1.5$ MW $\to \Delta 0$ MW at time $t_4 = 140s$.

Disturbance Rejection: We simulate the response to a change of the cooling water temperature, where the temperature change is modeled as the step response of a first order lag element with time constant $T = 50$s and gain $K = -2$.

The simulation for the set point change and the disturbance rejection are shown in Fig. 6 and Fig. 7, respectively. Consider the results of the set point change first (Fig. 6a). It is evident that set point changes around the operation

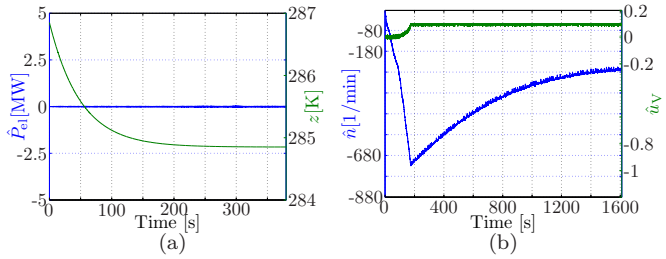

Fig. 7. Results for the disturbance rejection: (a) blue curve shows the simulated electric power, green curve shows the disturbance signal (b) inputs of the system; blue curve corresponds to the speed of the feedwater pump, green curve corresponds to the valve position.

point ($\pm\Delta 1$ MW) can be achieved by the proposed controller. If the set point changes from $\Delta 1$ MW $\rightarrow \Delta 1.5$ MW the trajectory tracking is less accurate. An explanation for this can be found in Fig. 6b, which shows the inputs of the system. The first two set point changes require only small variations of both inputs. However, if the set point changes from $\Delta 1$ MW to $\Delta 1.5$ MW, the valve fully opens and runs into saturation at the upper limit. To further increase the generated power, the controller drastically increases the speed of the feed water pump. Note that the rate constraints limit the changes in the speed of the feed water pump.

Results for the disturbance rejection are shown in Fig. 7. The cooling water temperature decreases aperiodically, cf. green curve in Fig. 7a. The controller rejects the disturbance and the electrical output remains approximately constant. The resulting inputs are shown in Fig. 7b.

In both Fig. 6a and Fig. 7a small oscillations of the generated power P_{el} can be observed. These oscillations result, since a simple generator model with damping constant $d_e = 0.3$ is used here. The oscillations are very small compared to the *nominal* generator output. The amplitude of the oscillations stays well below 1% of the nominal power in all simulations. As a result the control inputs $\hat{u}_{\mathrm{V}}$ and $\hat{n}$ also show small oscillations to compensate the oscillations of the generated power P_{el}.

6. SUMMARY AND OUTLOOK

We derived a nonlinear model for the steam cycle of a solar power plant, estimated unknown model parameters by applying nonlinear least squares estimation to measured data, verified the resulting model with independent data, and proposed and successfully tested a linear MPC controller for this system in simulations. The model represents the behavior of the real-world system very accurately over a wide range of operation. Specifically, the largest root mean squared error was observed for the outlet pressure p_4 and was lower than 1.5%. The proposed model predictive controller, despite being linear, is able to regulate the nonlinear system to a given output trajectory and provided good disturbance rejection.

Future work will address the implementation of the MPC controller for the control of a solar power plant or parts thereof. In addition, the nonlinear model will be used for the optimal control of start-up and shut-down procedures.

REFERENCES

Alduchov, O.A. and Eskridge, R.E. (1996). Improved Magnus form approximation of saturation vapor pressure. *Journal of Applied Meteorology and Climatology*, 35, 601–609.

Camacho, E.F., Rubio, F.R., Alvarado, I., and Limon, D. (2010). Control of solar power systems: a survey. In *Proceedings of the 9th International Symposium on Dynamics and Control of Process Systems*, 817 – 822.

Camacho, E.F., Rubio, F.R., Berenguel, M., and Valenzuela, L. (2007a). A survey on control schemes for distributed solar collector fields Part I: Modeling and basic control approaches. *Solar Energy*, 81, 1240–1251.

Camacho, E.F., Rubio, F.R., Berenguel, M., and Valenzuela, L. (2007b). A survey on control schemes for distributed solar collector fields Part II: Advanced Control Approaches. *Solar Energy*, 81, 1252–1272.

Chapman, S.J. (2012). *Electric Machinery Fundamentals*. McGraw Hill.

Grote, W. (2009). *A contribution to model based control of extraction steam turbines (In German)*. Ph.D. thesis, Ruhr-Universität Bochum.

Gülich, J.F. (2010). *Centrifugal Pumps*. Springer.

Incropera, F.P., DeWitt, D.P., Bergman, T.L., and Lavine, A.S. (2007). *Fundamentals of Heat and Mass Transfer*. Wiley & Sons, 6th edition.

Jost, M., Grote, W., Möllenbruck, F., and Mönnigmann, M. (2014). Plant-wide control of a parabolic trough power plant with thermal energy storage. In *Proceedings of the 19th IFAC World Congress*, 419–425.

Leonow, S. and Mönnigmann, M. (2013). Soft sensor based dynamic flow rate estimation in low speed radial pumps. In *Proceedings of the European Control Conference 2013*, 778–783.

Maciejowski, J.M. (2002). *Predictive Control with Constraints*. Prentice Hall.

Sonntag, R.E. and Van Wylen, G.J. (1971). *Introduction to Thermodynamics: Classical and Statistical*. John Wiley & Sons, Inc.

Wagner, W. and Kretzschmar, H.J. (1997). *International Steam Tables: Properties of Water and Steam based on the Industrial Formulation IAPWS-IF97*. Springer, 2nd edition.

Appendix A. NONLINEAR ODE

The model summarized in (24) reads

$$\dot{x} = \begin{pmatrix} \frac{c^2}{V_2} \cdot (\dot{m}_2 - \dot{m}_{LF} - \dot{m}_{2.2} - \dot{m}_3) \\ \frac{c^2}{V_{\mathrm{C}}}(\dot{m}_3 - \dot{m}_{3,T} - \dot{m}_4) \\ x_4 \\ \frac{1}{\theta}(M_{\mathrm{I}} - M_{\mathrm{T}} \sin(x_3) - d_{\mathrm{e}} x_4) \\ \frac{2\dot{m}_w}{m_w}(z - x_5) + \frac{2}{m_w c_p} Q \\ \frac{\dot{m}_{\mathrm{P,o}}}{m_{\mathrm{P,o}}}(T_{\mathrm{P,i}} - x_6) - \frac{kA}{m_{\mathrm{P,o}} c} \Delta\vartheta_{\log}(x_6 - T_{\mathrm{w,i}}, T_{\mathrm{P,i}} - T_{\mathrm{w,o}}) \\ \frac{c^2}{V_{\mathrm{i}}}(\dot{m}_{PH} - \dot{m}_{\mathrm{P,o}}) \\ \frac{2\dot{m}_{\mathrm{E,o}}}{m_{\mathrm{E,o}}}(T_{\mathrm{E,i}} - x_8) - \frac{2kA}{m_{\mathrm{E,o}} c_{\mathrm{p}}} \Delta\vartheta_{\log}(x_8 - T_{\mathrm{w,i}}, T_{\mathrm{E,i}} - T_{\mathrm{w,o}}) \\ \frac{c^2}{V_{\mathrm{E}}}(\dot{m}_{E,i} - \dot{m}_{\mathrm{E,o}}) \end{pmatrix},$$

$$y = M_{\mathrm{T}} \sin(x_3) 2\pi f_0,$$

where the mass flows $\dot{m}_2$, $\dot{m}_{LF}$, $\dot{m}_{2.2}$, $\dot{m}_3$, $\dot{m}_{3.T}$, $\dot{m}_4$, $\dot{m}_{PH}$, $\dot{m}_{\mathrm{P,o}}$, $\dot{m}_{\mathrm{E,o}}$ are calculated with (2), (4), (7), (2), (6), (11), (8), (21), (21) respectively. We use indices "i" and "o" for inlet and outlet, respectively. Note that both $\dot{m}_{\mathrm{E,o}}$ and $\dot{m}_{\mathrm{P,o}}$ are calculated with the same equation but different parameters. Moreover, Q and kA are calculated with (12) and (13), respectively. Finally, $M_{\mathrm{I}} = {}^{P}/_{2\pi f_0}$, where the thermal power P follows from (9). Both Δh_{HP} and Δh_{NP} in (9) can be calculated with Alg. 3.